doi:10.1016/j.jmb.2010.10.056 J. Mol. Biol. (2011) 405, 926–938

Contents lists available at www.sciencedirect.com

Journal of Molecular Biology

journal homepage: http://ees.elsevier.com.jmb

Tuning Riboswitch Regulation through Conformational Selection

Ross C. Wilson[1,2], Angela M. Smith[2,3], Ryan T. Fuchs[2,3], Ian R. Kleckner[1,2], Tina M. Henkin[2,3] and Mark P. Foster[1,2*]

[1]*Department of Biochemistry, Ohio State University, Columbus, OH 43210, USA*
[2]*Center for RNA Biology, Ohio State University, Columbus, OH 43210, USA*
[3]*Department of Microbiology, Ohio State University, Columbus, OH 43210, USA*

Received 25 August 2010; received in revised form 27 October 2010; accepted 28 October 2010
Available online 12 November 2010

Edited by D. E. Draper

Keywords:
NMR spectroscopy; isothermal titration calorimetry; gene regulation; preexisting equilibrium; riboswitch

The S_{MK} box riboswitch, which represents one of three known classes of *S*-adenosylmethionine (SAM)-responsive riboswitches, regulates gene expression in bacteria at the level of translation initiation. In contrast to most riboswitches, which contain separate domains responsible for ligand recognition and gene regulation, the ligand-binding and regulatory domains of the S_{MK} box riboswitch are coincident. This property was exploited to allow the first atomic-level characterization of a functionally intact riboswitch in both the ligand-bound state and the ligand-free state. NMR spectroscopy revealed distinct mutually exclusive RNA conformations that are differentially populated in the presence or in the absence of the effector metabolite. Isothermal titration calorimetry and *in vivo* reporter assay results revealed the thermodynamic and functional consequences of this conformational equilibrium. We present a comprehensive model of the structural, thermodynamic, and functional properties of this compact RNA regulatory element.

Introduction

Riboswitches are regulatory RNA elements that are usually located in the 5′ untranslated regions of certain mRNAs. These elements directly respond to environmental signals to regulate the expression of cis-encoded genes without the requirement for additional regulatory factors or proteins.[1–3] Riboswitches are classified based on the environmental signal that they recognize and on the conserved sequence and structural elements involved in signal recognition. Most riboswitches discovered to date regulate genes involved in the metabolism and transport of vitamins, amino acids, nucleic acids, enzymatic cofactors, and metal ions.[2] In many instances, the ligand recognized by an individual riboswitch is a metabolic end-product or intermediate in the pathway regulated by that riboswitch. While most known riboswitches have been identified in bacteria, one class of riboswitch, the THI box, has been found in all three domains of life,[4,5] demonstrating the prevalence of these regulatory RNAs.

Signal recognition by riboswitch RNAs typically results in a structural rearrangement that alters the efficiency of expression of an adjacent open reading frame. The two most common riboswitch mechanisms involve regulation at the level of premature termination of transcription or translation initiation. Riboswitches that affect transcription termination undergo a conformational switch that either

*Corresponding author. E-mail address: foster.281@osu.edu.

Abbreviations used: SAM, *S*-adenosylmethionine; SD, Shine–Dalgarno; ITC, isothermal titration calorimetry; 1D, one-dimensional; NOE, nuclear Overhauser enhancement; NOESY, NOE spectroscopy; 2D, two-dimensional; SAXS, small-angle X-ray scattering; HSQC, heteronuclear single-quantum coherence.

stabilizes or destabilizes the helix of an intrinsic transcription terminator. Translational regulation utilizes a conformational change that affects the accessibility of the Shine–Dalgarno (SD) sequence, which is the binding site for the 30S ribosomal subunit. In each of these mechanisms, the riboswitch element is predicted to favor one of two mutually exclusive alternate conformations, depending on the presence or the absence of the specific effector molecule or physiological signal to which it responds.

The S_{MK} box riboswitch is one of three known riboswitch classes that bind the enzymatic cofactor *S*-adenosylmethionine (SAM) (S box/SAM-I, SAM-II, and S_{MK} box/SAM-III).[6–8] Each of the SAM-binding riboswitches forms a unique ligand-binding pocket (characterized by conserved sequence elements and structural features) that specifically accommodates SAM.[9–11] All known S_{MK} box elements regulate the expression of the *metK* gene, which encodes SAM synthetase, the enzyme responsible for the production of SAM from adenosine and methionine.[7,12] This riboswitch element regulates *metK* expression at the level of translation initiation through sequestration of a portion of the SD sequence by pairing with an upstream anti-SD sequence (Fig. 1; Supplemental Fig. 1a and b). The anti-SD–SD interaction is stabilized in the presence of SAM, resulting in SAM-dependent inhibition of ribosome binding.[12]

While most riboswitch RNAs have a modular architecture composed of two separate domains (i.e., an aptamer domain for signal recognition and a regulatory domain), the S_{MK} box riboswitch has a simpler architecture that utilizes a single domain for both ligand binding and gene regulation.[10,12] This compact design facilitates high-resolution structural investigations using the complete riboswitch element. The crystal structure of a 53-nt minimal S_{MK} box element (based on the *Enterococcus faecalis metK* sequence) in complex with SAM revealed that the RNA forms a Y-shaped arrangement with SAM located in the center of a three-way junction at the intersection of helices P1, P2, and P4 (Fig. 1b; Supplemental Fig. 2).[10] Pairing interactions in each of these helical domains are required for SAM binding, and formation of helices P1 and P4 results in sequestration of residues 88–92, which constitute the *metK* SD sequence, providing a structural basis for SAM-dependent translational repression. These results verified the prediction that the S_{MK} box riboswitch assumes a single-domain architecture and demonstrated that the SD sequence is directly involved in SAM binding through base-specific contacts.

There is less available evidence for the ligand-free conformation of the S_{MK} box riboswitch. Based on phylogenetic analysis, helices P1, P2, and P4 were predicted to be absent, and another helix (referred to here as P0) was predicted to be formed in the absence of SAM (Fig. 1a).[7] Helix P0 is predicted to comprise residues 13–20 and 68–75 (relative to the predicted *E. faecalis metK* transcription start site), which include nucleotides that overlap helices P2 and P4 in the ligand-bound conformation. Therefore, the two conformations (ligand bound and unbound) are mutually exclusive, and stabilization of helices P2 and P4 upon SAM binding is predicted to disrupt helix P0. Results from a variety of experiments (e.g., enzymatic probing, RNase H cleavage assays, and 30S ribosomal toeprinting) provide evidence that the RNA assumes an alternate conformation in the absence of ligand and exhibits secondary structural features consistent with the model.[7,12]

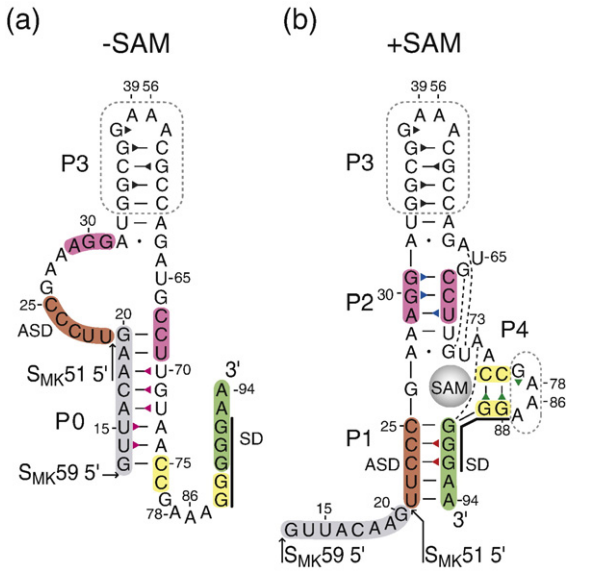

Fig. 1. Secondary structure of the S_{MK} box riboswitch. Previously proposed SAM-free (a) and SAM-bound (b) secondary structure models of the S_{MK} box, represented as the S_{MK}59 construct used in this study. The S_{MK}51 construct lacks the eight 5′ nucleotides (gray). The boxed regions were truncated from hypervariable regions in the naturally occurring *E. faecalis metK* sequence. Numbering is based on the *E. faecalis metK* sequence and is discontinuous at the engineered tetraloops. The SD sequence is marked with a black line. Base pairs observed in the crystal structure[10] are marked: dash line, Watson–Crick; dotted line, noncanonical; broken line, extrahelical. Triangles represent assigned imino protons and are colored corresponding to the labels in Figs. 2 and 3.

In the current study, we used NMR spectroscopy to investigate the pairing interactions of the S_{MK} box riboswitch in the presence and in the absence of SAM. We show that a 51-nt minimal construct (S_{MK}51; Fig. 1) lacking residues 13–20 at the 5′ end of the RNA favors a conformation resembling the ligand-bound state even in the absence of SAM. Inclusion of these eight additional 5′ nucleotides to

generate a 59-nt construct (S_{MK}59; Fig. 1) resulted in an RNA that is capable of assuming two alternate conformations depending on the presence of SAM. These results validate the predicted secondary structural features of the S_{MK} box riboswitch in each conformational state and demonstrate that residues at the 5′ end of the element (which are not required for ligand binding) are essential for the stabilization of the ligand-free conformation. Moreover, we describe in detail the thermodynamic and functional implications of the ability of the riboswitch to adopt two distinct and mutually exclusive structures by isothermal titration calorimetry (ITC) and *in vivo* reporter assays. Taken together, our results provide new insights into the interplay between structure and function in ligand-sensing regulatory RNA elements.

Results

NMR spectroscopy of SAM-bound S_{MK}51 and S_{MK}59

S_{MK}51, the initial RNA construct used for NMR studies (Fig. 1), consists of 51 nt equivalent to the minimal aptamer sequence used to determine the crystal structure of the SAM-bound S_{MK} box (Supplemental Fig. 2).[10] Because of its known secondary and tertiary structures, the SAM-bound state of S_{MK}51 served as a starting point for the interpretation of NMR spectra. NMR structural characterization of the two S_{MK} box riboswitch constructs is based primarily on the detection of exchangeable imino proton resonances of the 51-nt or 59-nt RNAs. These resonances are direct reporters of base-pairing interactions, since the signals can be observed only if the protons are protected from solvent, while shifts in peak position reflect changes in the local chemical environment, including (but not limited to) conformational changes. The S_{MK}51 RNA binds SAM more tightly than does the 106-nt wild-type sequence (corresponding to residues 15–118; see Supplemental Fig. 1) in a size-exclusion filtration assay (Supplemental Fig. 3), indicating that it is fully active in SAM binding.

The one-dimensional (1D) proton spectrum of S_{MK}51 in the presence of a 10% stoichiometric excess of SAM reveals 14 imino resonances (Fig. 2a). The two overlapped signals upfield of 11 ppm can be assigned to the two guanines in tetraloops that cap helices P3 and P4 because these iminos have diagnostic chemical shifts.[13,14] The remaining 12 signals arise from imino protons participating in helical base pairs. Analysis of the SAM-bound crystal structure suggests that 21 imino protons participate in base pairs (none of which is base-paired to the SAM ligand). Comparison to NMR data indicates that seven of the crystallographically observed base pairs do not yield observable imino resonances, likely due to local "breathing" motions

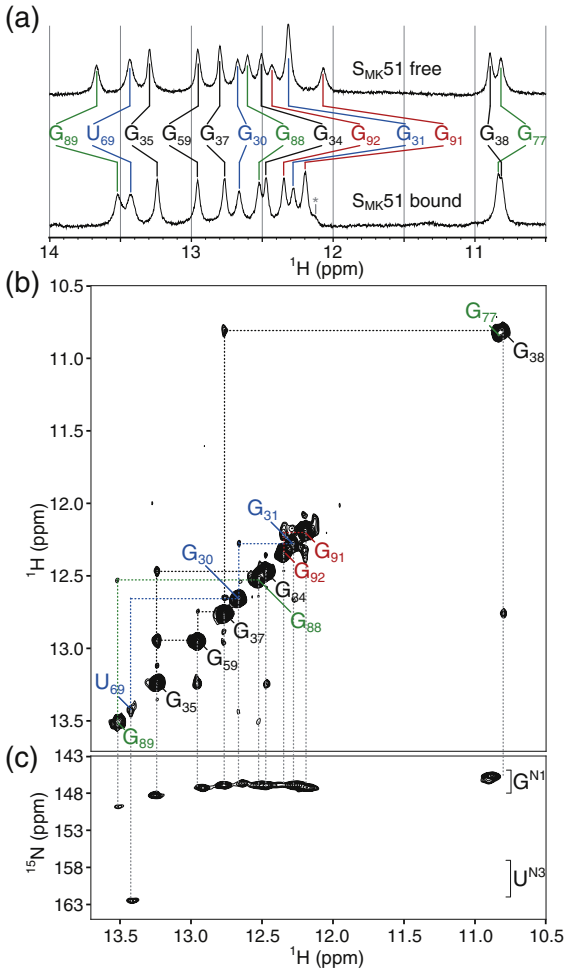

Fig. 2. NMR spectra of S_{MK}51 at 4 °C reveal a folded aptamer domain. (a) The imino region of the 1D ^{1}H spectra of SAM-free (top) or SAM-bound (bottom) S_{MK}51. The number of observed resonances indicates the number of imino protons protected from solvent exchange (e.g., via base-pairing), while changes in peak position between states reflect a difference in the chemical environment of a given proton. An unassigned resonance is marked by an asterisk. (b) Imino region of the ^{1}H–^{1}H NOESY spectrum of SAM-bound S_{MK}51. Signals along the diagonal are analogous to those observed in the 1D spectra. Off-diagonal cross-peaks reflect through-space magnetization transfer between two protons within ~5 Å of each other. In the context of regular nucleic acid structure, protons whose signals are serially connected by cross-peaks belong to a continuous region of secondary structure. NOE spin networks of helical regions are labeled: P1, red; P2, blue; P3, black; P4, green (represented as color-coded triangles in Fig. 1b). (c) ^{1}H–^{15}N HSQC spectrum of SAM-bound S_{MK}59, whose imino spectra are nearly identical with those of SAM-bound S_{MK}51. The ^{15}N chemical shift allows assignment of nucleotide type (G or U).

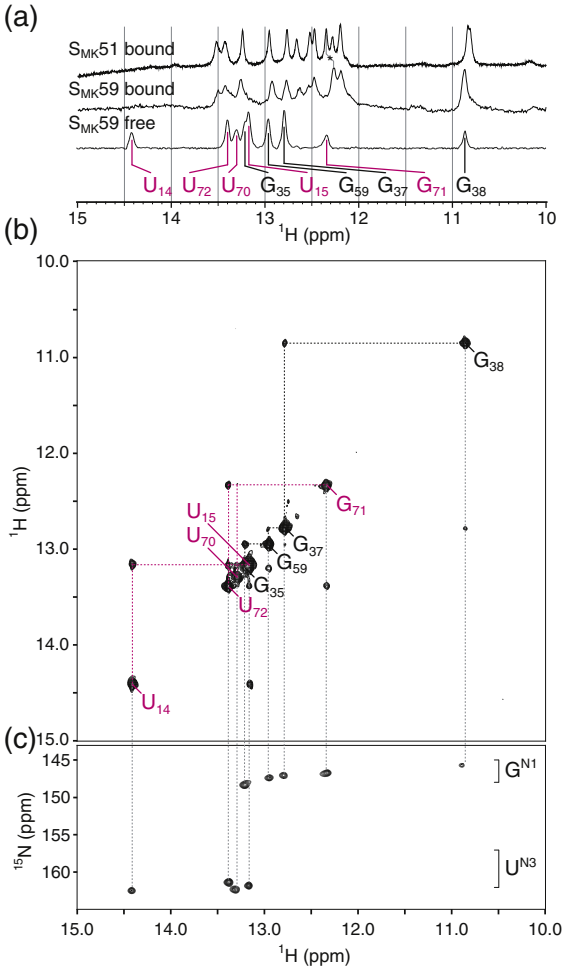

Fig. 3. NMR spectra of S_{MK}59 at 4 °C reveal a novel fold in the absence of ligand. (a) The imino region of the 1D ^{1}H spectra of SAM-bound S_{MK}51 (top), SAM-bound S_{MK}59 (middle), or SAM-free S_{MK}59 (bottom). Similarity of chemical shifts indicates near-identical structures for the SAM-bound constructs. A resonance shifted between the two bound states was used for the assignment of G92 and is marked with an asterisk. The helix P3 spin network is labeled in black as in Fig. 2; signals from helix P0 are labeled in magenta (represented as color-coded triangles in Fig. 1a). (b) Imino region of the ^{1}H–^{1}H NOESY spectrum of SAM-free S_{MK}59. The helix P3 spin network is largely unperturbed compared to the SAM-bound state, but a novel spin network corresponding to helix P0 is detected. (c) ^{1}–^{15}N HSQC spectrum of SAM-free S_{MK}59 allows assignment of nucleotide type.

in the RNA that deprotect the protons from solvent or otherwise lead to resonance broadening.

S_{MK}51 lacks 8 nt at the 5′ end (Fig. 1) that are hypothesized to participate in the formation of helix P0 in the absence of SAM; this is supported by the observation that a P0-containing conformation is not adopted by ligand-free S_{MK}51 (see the text). A second construct, S_{MK}59, contains these additional 8 nt and was therefore predicted to be able to form the P0 helix in the absence of SAM. No additional signals were expected in the imino region of SAM-bound S_{MK}59, since the additional nucleotides unique to this RNA are predicted to be single stranded and deprotected from solvent in this state. Accordingly, the spectra of SAM-bound S_{MK}59 are nearly identical with those of SAM-bound S_{MK}51 (Fig. 3a, top and middle spectra). Four spin networks in S_{MK}51 and S_{MK}59 could be confidently assigned to bases in helices P1, P2, P3, and P4 using nuclear Overhauser enhancement (NOE) spectroscopy (Fig. 2; see Supplemental Results). These networks correspond to the four helical regions observed in the crystal structure.

NMR spectroscopy of SAM-free S_{MK}51

The NMR spectra of ligand-free S_{MK}51 were recorded to investigate the structure of this RNA in the absence of SAM. At 4 °C, the NMR spectra of SAM-free S_{MK}51 are similar to those of the SAM-bound RNA (Fig. 2; Supplemental Fig. 4). This similarity suggests that the global structure is unperturbed, while minor chemical shift perturbations reflect the altered chemical environment near the binding pocket due to the absence of the ligand. In contrast, the NOE spectroscopy (NOESY) spectrum of SAM-free S_{MK}51 recorded at 25 °C shows an extensive loss of imino proton signals compared to that of SAM-bound S_{MK}51 at the same temperature (Supplemental Fig. 5). Under these conditions, spin networks from helices P1 and P4 in SAM-free S_{MK}51 were undetected, while helices P2 and P3 were largely intact. This observation reflects the reduced stability of the ligand-binding region of an otherwise unperturbed S_{MK}51 in the absence of SAM.

NMR spectroscopy of SAM-free S_{MK}59

In contrast to S_{MK}51, the ^{1}H–^{1}H NOESY spectrum of SAM-free S_{MK}59 reports the absence of all structural elements detected in the SAM-bound state, with the exception of helix P3, and the appearance of a new spin network containing 5 bp (Fig. 3b). Although the P3 helix resonances are subject to slight chemical shift perturbations, the data indicate that this helix remains intact, with the exception of the imino signal from G34, which is not observed. This suggests increased breathing in SAM-free S_{MK}59 brought about by the unfolding of the P2 helix, whose resonances are not observed. The new NOE spin network was revealed to contain a U·U·U·G·U pattern via a ^{1}H–^{15}N correlated spectrum (Fig. 3c); thus, this network was assigned to helix P0 (residues U14·U15·U72·G71·U70).

A two-dimensional (2D) ^{1}H–^{15}N correlated spectrum was used to confirm that the assigned P0 iminos participate in canonical Watson–Crick base

pairs (Supplemental Fig. 6). In light of weak diagnostic G71·U70 cross-peaks, ^{1}H–^{1}H NOESY spectra of model helices were used to verify the assignment of nucleotides in helix P0 (Supplemental Fig. 7). Taken together, these data reveal that the $S_{MK}59$ RNA adopts a unique fold in the absence of SAM; three of the helices (P1, P2, and P4) found in the SAM-bound structure are absent, and a new helix (P0) is formed.

Isothermal titration calorimetry

ITC was used to measure the binding affinities of the two S_{MK} box constructs for SAM at 15 °C. The ligand was titrated into either $S_{MK}51$ RNA or $S_{MK}59$ RNA (Fig. 4a and b). Data were fitted to a single-site binding model, yielding the following values: $S_{MK}51$, $\Delta H = -18.7 \pm 0.2$ kcal mol^{-1}, $K_d = 63 \pm 11$ nM, $\Delta S = -32.0 \pm 0.8$ cal K^{-1} mol^{-1} (Fig. 4a); $S_{MK}59$, $\Delta H = -10.7 \pm 0.3$ kcal mol^{-1}, $K_d = 400$ nM ± 78 nM, $\Delta S = -7.9 \pm 1.1$ cal K^{-1} mol^{-1} (Fig. 4b). Relative to $S_{MK}59$, $S_{MK}51$ exhibits a ~6-fold-higher affinity for SAM, consistent with the observation that the $S_{MK}51$ RNA binds SAM more efficiently than does the full-length *E. faecalis metK* sequence in filtration experiments (Supplemental Fig. 3).

Because the ligand-bound states of the $S_{MK}51$ and $S_{MK}59$ constructs contain similar spectroscopically indistinguishable binding sites (Fig. 3a), we attribute the observed differences in the SAM-binding affinities of $S_{MK}51$ and $S_{MK}59$ primarily to differences in the relative stabilities of their unliganded states. The NMR data report that in the absence of ligand, $S_{MK}51$ remains in a state similar to that adopted in the presence of SAM; this state, designated $PRIMED_{SMK}$, may represent a structural intermediate in which the RNA is *primed* for SAM binding. In contrast, the alternative structure adopted by $S_{MK}59$

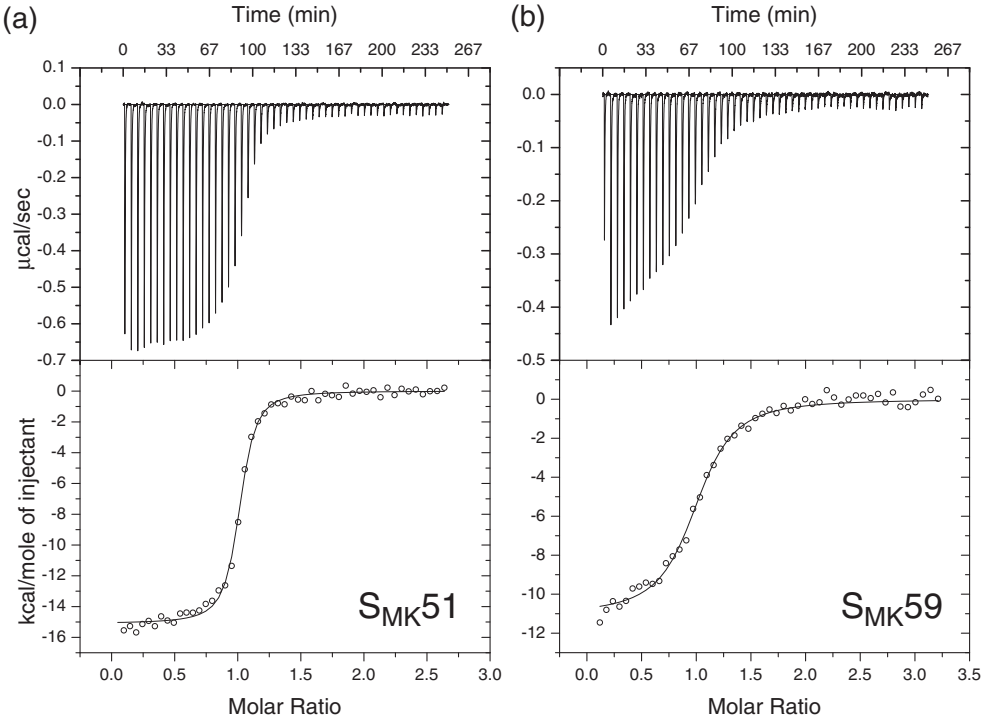

(c)

Fusion	P0-capable	-Met	+Met	Induction ratio
$S_{MK}51$	-	3.7 ± 1.2	0.34 ± 0.088	11 ± 1.0
$S_{MK}59$	+	37 ± 4.3	3.0 ± 0.45	13 ± 0.43
$S_{MK}20$-116	-	15 ± 2.6	4.8 ± 0.6	3.1 ± 0.13
$S_{MK}13$-116	+	119 ± 12	21 ± 2.3	5.8 ± 0.29

Fig. 4. ITC and *in vivo* assays with the S_{MK} box. (a) Thermogram generated upon the titration of SAM into $S_{MK}51$. Fitting to a one-site model reveals a ΔH of −18.7 ± 0.2 kcal mol^{-1} and a K_d of 63 ± 11 nM. (b) Analogous data for $S_{MK}59$, with a ΔH of −10.7 ± 0.3 kcal mol^{-1} and a K_d of 400 ± 78 nM. (c) Expression of P_{gly}–*metK*–*lacZ* fusions in *B. subtilis* during growth under high-SAM (+Met) or low-SAM (−Met) conditions. β-Galactosidase activities are expressed in Miller units. Induction ratio refers to β-galactosidase activity in cells grown in the absence of methionine divided by the activity in cells grown in the presence of methionine.

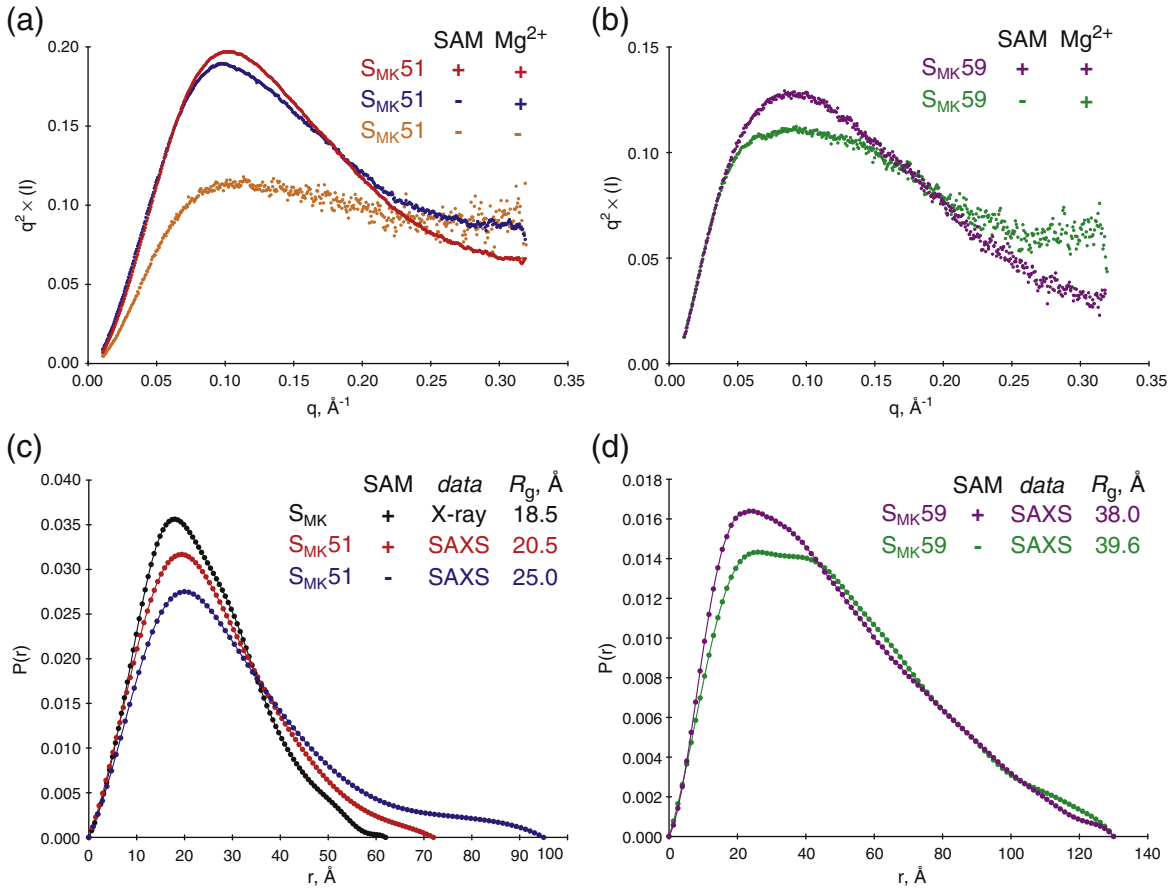

Fig. 5. SAXS analysis of the S_{MK} box in the presence and in the absence of ligand. (a) Kratky plots reveal an increased folding of $S_{MK}51$. An unfolded biopolymer is typified by a $q^2 \times (I)$ plateau at high-scattering angles ($q > 0.2$ Å^{-1}), and this character decreases upon the addition of Mg^{2+} (blue) and SAM (red). (b) SAM-associated folding can also be observed in Kratky plots of $S_{MK}59$ in the presence (purple) or in the absence (green) of SAM. (c) Intramolecular pair distribution functions for the S_{MK} box. A simulated curve was generated for the previously determined crystal structure of the 53-nt S_{MK} box bound to SAM (black) and is compared to curves resulting from a SAXS analysis of the 51-nt $S_{MK}51$ in solution (red, with SAM; blue, without SAM). Comparison of the radii of gyration R_g suggests that the solution conformation is less compact than that adopted in the crystal. The binding of SAM is associated with a compaction of the solution structure of $S_{MK}51$ based on the similar curve shapes and markedly different R_g values for free (25.01 Å; blue) *versus* bound (20.52 Å; red). (d) Comparison of SAXS-derived pair distribution curves for $S_{MK}59$ with (purple) and without (green) SAM reveals a noteworthy change in the overall shape of the molecule. While the SAM-bound state generates a curve resembling those from the SAM-bound $S_{MK}51$ species (c), the bimodal distribution in the absence of SAM is indicative of a two-lobed structure as might be expected for the ISO_{SMK} state, which is composed of two helical segments connected by a single-stranded region.

in the absence of SAM, designated ISO_{SMK}, must undergo conformational isomerization in order to bind the ligand.

Because the secondary structure of the ISO_{SMK} state is incompatible with RNA–SAM contacts in the $BOUND_{SMK}$ state, we judged the isomerization between the ISO_{SMK} state and the $BOUND_{SMK}$ state of $S_{MK}59$ as most likely to occur through conformational sampling via a preexisting equilibrium.[15] If SAM can bind only to one of the two equilibrating $S_{MK}59$ states (i.e., mandatory coupling),[16] the weaker effective affinity K_{eff} of $S_{MK}59$ can be quantitatively linked to the thermodynamic equilibrium K_{ISO} between the isomerizing states:

$$ISO_{SMK} \underset{K_{ISO}}{\rightleftharpoons} PRIMED_{SMK} + SAM \overset{K_a}{\rightleftharpoons} BOUND_{SMK} \quad (1)$$

$$K_{eff} = \frac{K_a}{1 + K_{ISO}} \quad (2)$$

where ISO_{SMK} is the P0-containing state observed in SAM-free $S_{MK}59$ (Fig. 6a, left), $PRIMED_{SMK}$ is the

binding-ready unliganded state observed in SAM-free S_{MK}51 (Fig. 6a, center), and $BOUND_{SMK}$ is the SAM-bound state observed in both constructs (Fig. 6a, right). K_a in Eqs. (1) and (2) is the affinity of the *primed* structure for SAM and is likely to be approximated well by the affinity of S_{MK}51 for SAM. K_{eff} in Eq. (2) is the effective affinity when the free state is subjected to conformational isomerization (i.e., $K_{ISO}>0$); this is approximated by the affinity of S_{MK}59 for SAM. Via this analysis, we find that K_{ISO} is ~5.3, which implies that under the conditions sampled, ~80% of SAM-free S_{MK}59 exists in the ISO_{SMK} conformation, while the remaining ~20% adopts an ensemble of conformations approximating the *primed*-like species. Simulated ITC data are consistent with this interpretation (Supplemental Fig. 8; see also Supplemental Results). Thus, the conformational equilibrium present in the switching-competent S_{MK}59 construct can be seen to have the following thermodynamic consequences compared to the switching-incompetent S_{MK}51 construct: (1) populating the competing structure in the ligand-free state necessarily decreases the net affinity of the RNA for its ligand; (2) binding enthalpy gain is reduced, at least in part, by the cost of breaking hydrogen bonds in helix P0; and (3) the entropic penalty for binding is reduced by the fewer degrees of freedom lost in rearranging the structured RNA (S_{MK}59) compared to ordering the disordered one (S_{MK}51).

In vivo riboswitch activity assays

To investigate the effect of the deletion of the 5′ residues on SAM-dependent repression *in vivo*, we compared four *metK–lacZ* translational fusion constructs incorporating varying S_{MK} box sequences. Two fusion constructs contained the S_{MK}51 and S_{MK}59 sequences and are named accordingly. Another pair of fusion constructs was based on the naturally occurring *E. faecalis* S_{MK} box; these constructs are named S_{MK}13–116 and S_{MK}20–116, respectively (Supplemental Fig. 1). The fusion constructs S_{MK}59 and S_{MK}13–116 contain the residues required for the formation of helix P0 (Fig. 1a), while S_{MK}51 and S_{MK}20–116 do not. Fusions were integrated into the chromosome of *Bacillus subtilis* strain BR151, a methionine auxotroph in which intracellular SAM pools can be modulated via the presence of methionine in the growth media.[17] In this strain, a *metK–lacZ* fusion corresponding to residues 15–118 exhibits a high expression when SAM pools are low and a ~5-fold repression when SAM levels are high.[7] Comparison of fusions corresponding to the wild-type *E. faecalis metK* sequence either containing (S_{MK}13–116) or lacking (S_{MK}20–116) the 5′ side of the P0 helix showed that while both were capable of SAM-dependent repression, the ability to form the P0 helix resulted in a higher expression during growth under both high-SAM conditions and low-SAM conditions (Fig. 4c). A similar pattern was observed for the model S_{MK}51 and S_{MK}59 RNAs, which exhibited a lower expression than the full-length *E. faecalis metK* constructs under both high-SAM conditions and low-SAM growth conditions, consistent with a higher affinity for SAM. These results are consistent with the model that the P0 helix stabilizes the SAM-free form and that absence of the helix facilitates the formation of the SAM-bound conformation, resulting in decreased expression (Figs. 4c and 6).

Small-angle X-ray scattering

To investigate the overall shape of the RNA molecules in various states, we recorded small-angle X-ray scattering (SAXS) data for S_{MK}51 and S_{MK}59 in the absence and in the presence of SAM. S_{MK}51 was also examined in the absence of Mg^{2+} and SAM. Guinier analysis shows potential moderate aggregation of the S_{MK}51 sample in the absence of SAM, while the other samples appear well behaved (Supplemental Fig. 9). Kratky plots were used to assess the relative foldedness of the various states. Increased folding is observed upon addition of 5 mM Mg^{2+} to S_{MK}51, with continued folding in the presence of SAM (Fig. 5a). Intramolecular distance pair distribution histograms (Fig. 5c) reveal a similar but less compact structure for S_{MK}51 in the absence of SAM compared to when the ligand is bound. These results are consistent with partial unfolding between the proposed $BOUND_{SMK}$ state and the proposed $PRIMED_{SMK}$ state (Fig. 6). Free and bound solution states of S_{MK}51 have a radius of gyration greater than that estimated based on the crystal structure of the slightly larger 53-nt S_{MK} box RNA used for crystallization,[10] suggesting a less compact structure in solution. This is consistent with the observation that not all crystallographically inferred hydrogen bonds give rise to observable imino proton resonances in NMR spectra.

Kratky plots reveal that S_{MK}59 also becomes more well folded in the presence of SAM (Fig. 5b). In contrast to S_{MK}51, the intramolecular distance pair distribution histograms for S_{MK}59 reveal a marked change in the structure of the RNA in response to SAM binding (Fig. 5d). In the presence of SAM, the S_{MK}59 histogram is roughly Gaussian, with a maximum at ~20 Å, consistent with the roughly prolate spheroidal $BOUND_{SMK}$ state (Fig. 6). In the absence of SAM, the S_{MK}59 pair distribution is bimodal with maxima at ~25 Å and ~40 Å; this is consistent with the rearrangement of the RNA into the ISO_{SMK} conformation, whose two helical regions (separated by poorly structured single-stranded RNA) would give rise to a bimodal distribution. Although we expect the minor population of

$PRIMED_{SMK}$ molecules present in solution to also contribute to the net scattering profile, the data clearly indicate the adoption of a significantly more extended conformation upon removal of SAM.

Using SAXS data, we generated an ab initio three-dimensional reconstruction of SAM-bound $S_{MK}51$. This model exhibits the same size and general features of the previously determined S_{MK} box crystal structure and verifies that the global fold of SAM-bound $S_{MK}51$ in solution resembles that observed in the crystal[10] (Supplemental Fig. 11).

Discussion

The previously determined crystal structure of the S_{MK} box bound to SAM[10] (Supplemental Fig. 2) reveals the structural details of ligand recognition, but does not address the conformational changes required for the RNA to fulfill its role in gene regulation. To date, no high-resolution structural study has characterized a riboswitch containing the aptamer and regulatory domains in both the ligand-free conformation and the ligand-bound conformation, which have opposing influences on gene regulation and are mutually exclusive. Several NMR and crystallographic studies have compared the ligand-free and ligand-bound states of isolated aptamer domains that lack residues to promote competing structures and in turn detected changes ranging from a minor rearrangement of the active site[18,19] to larger impacts on tertiary structure and dynamics.[20–24] Here we utilize two constructs to probe the role of competing conformations in riboswitch gene control: $S_{MK}51$, which favors a bound-like conformation even in the absence of SAM, and $S_{MK}59$, which is capable of switching between regulatory states.

The nonswitching construct $S_{MK}51$ corresponds to the RNA whose crystal structure was previously solved in a ligand-bound state and is shown via NMR spectroscopy to adopt a secondary structure in solution resembling that observed in the crystal.[10] The SAM-bound solution structure of $S_{MK}51$ is consistent with the crystal structure based on imino proton assignments obtained using 2D ^{1}H–^{1}H NOESY spectroscopy (Fig. 2b). Furthermore, an ab initio SAXS reconstruction verifies that the overall structure of SAM-bound $S_{MK}51$ is extremely similar to that of the S_{MK} box crystal structure (Supplemental Fig. 11). However, fewer imino proton resonances were observed than might be expected from the crystallographically observed base-pairing, implying dynamics that result in exchange with solvent and/or resonance broadening. Indeed, a comparison of SAXS data for $S_{MK}51$ and scattering data simulated from coordinates of the S_{MK} box crystal structure is consistent with a less compact structure in solution than in the lattice (Fig. 5c). In the absence of ligand, the structure of this switching-incompetent RNA is largely unchanged at 4 °C based on detection of the same NOE spin networks (Supplemental Fig. 4a) and observation of only small chemical shift perturbations with respect to the bound state (Fig. 2a), characteristic of local changes expected upon ligand removal. At higher temperatures (25 °C), the RNA undergoes a loss of secondary structure in helices near the binding pocket (P1 and P4), with only helix P3 retaining a bound-like structure (Supplemental Fig. 5). The NMR data are supported by the SAXS-based observation of a less well-folded and less compact $S_{MK}51$ in the absence of ligand (Fig. 5a and c). These results are generally consistent with the range of findings from previous studies of riboswitch aptamer domain structure, from minor changes localized to the ligand-binding site[18,19] (observed at 4 °C in $S_{MK}51$) to a larger-scale loss of structure in the absence of ligand[24,25] (observed at 25 °C in $S_{MK}51$).

To investigate conformational rearrangement at the crux of riboswitch function, we utilized the $S_{MK}59$ construct, which contains eight 5′ nucleotides necessary for the formation of helix P0, the paired region predicted from phylogenetic analysis to be formed in the SAM-free state (Fig. 1a).[7] Near-identical NMR spectra of ligand-bound states confirm that the conformation of the $S_{MK}59$–SAM complex is equivalent to that of $S_{MK}51$ (Fig. 3a), as would be expected, since the single-stranded nucleotides exclusive to $S_{MK}59$ should not produce detectable imino proton signals. In contrast, the spectra of ligand-free $S_{MK}59$ reveal an extensive change in the RNA structure relative to the SAM-bound state (Fig. 3b). Although helix P3 remains largely unperturbed, the three remaining imino spin networks near the SAM-binding pocket are replaced with a novel 5-nt spin network corresponding to helix P0 (Fig. 3; Supplemental Fig. 6). As with the SAM-bound state, the SAM-free state is less well folded than would be predicted based on an examination of the sequence; P0 could potentially comprise 8 bp, yet only 5 bp are detected via NMR. This reconfiguration upon ligand binding is corroborated by SAXS data revealing globally distinct conformations of $S_{MK}59$ in the presence or in the absence of SAM (Fig. 5d). $S_{MK}59$, therefore, is revealed to be a minimal riboswitch that is capable of adopting two mutually exclusive, biologically relevant folds in response to its ligand.

Three states of the S_{MK} riboswitch were observed via NMR: (1) a SAM-free "on"-state, where the SD sequence is exposed (ISO_{SMK}; Fig. 6a, left); (2) a potential intermediate state, which consists of a poorly folded structure resembling the SAM-bound state ($PRIMED_{SMK}$; Fig. 6a, center); and (3) a SAM-bound "off"-state, which is well folded and resembles the crystal structure ($BOUND_{SMK}$; Fig. 6a, right). Consideration of these states is useful in interpreting thermodynamic data obtained via ITC

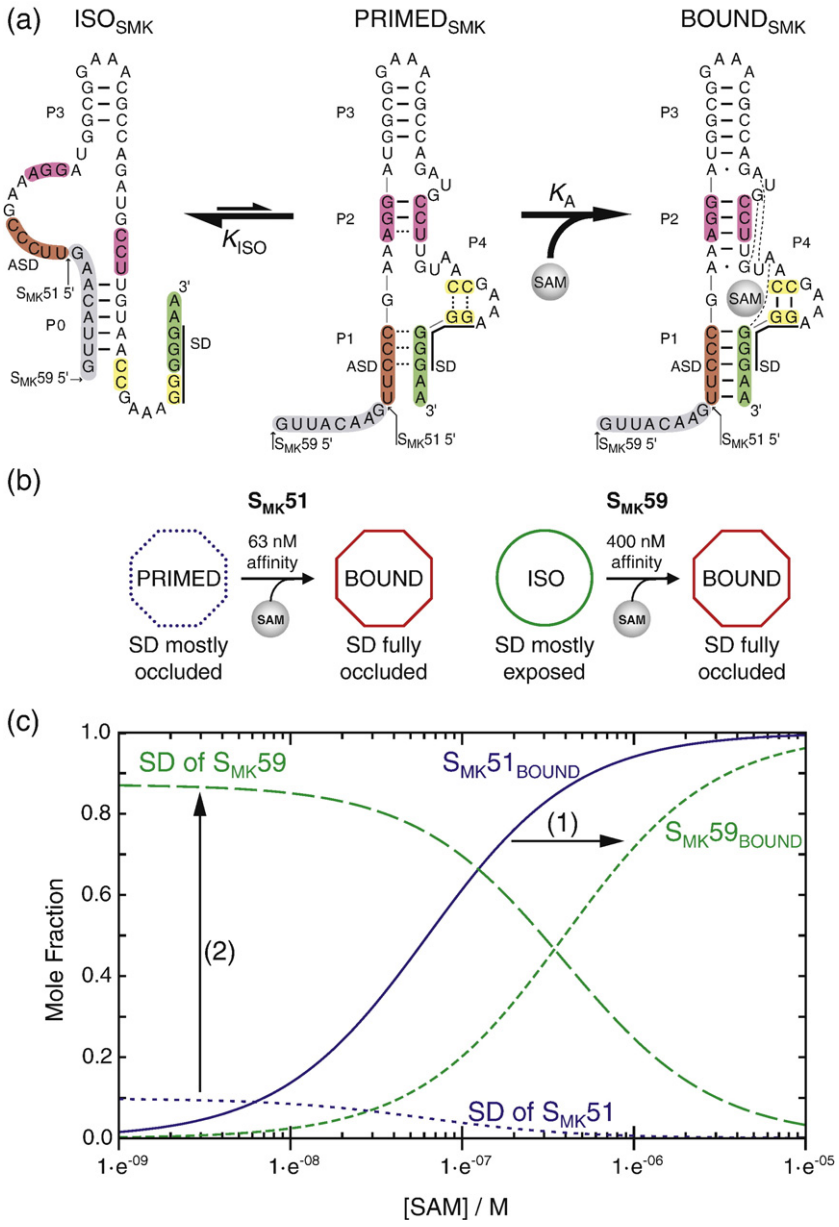

Fig. 6. Model of S_{MK} box structural transitions in response to SAM. (a) Observed conformations of the S_{MK} box. Left: The free state observed in SAM-free S_{MK}59 via NMR, with accessible SD sequence. Center: The poorly folded state observed via NMR in SAM-free S_{MK}51 (which is missing the eight 5′ nucleotides shown here in gray), with a partially accessible SD sequence. Right: The well-folded SAM-bound state with occluded SD sequence, observed in ligand-bound S_{MK}51 and S_{MK}59, and the previously determined crystal structure. Hydrogen bonds are represented as lines, as observed via NMR for ISO_{SMK} and $PRIMED_{SMK}$, while hydrogen bonds expected based on the crystal structure[10] are shown for $BOUND_{SMK}$. Broken lines in the $PRIMED_{SMK}$ state represent transiently formed base pairs as detected via NMR. (b) A schematic representing the transitions observed in ITC for S_{MK}51 or S_{MK}59 and how the analogous constructs behave while undergoing similar transitions inside the cell, as measured by β-galactosidase reporter assays. (c) Effect of the alternatively folded conformation on the populations of riboswitch conformations. The SAM dependence of molecular species is simulated from Eqs. (2) and (3), which describe the fractional populations of the SAM-bound species ($S_{MK}51_{BOUND}$ and $S_{MK}59_{BOUND}$) and the effective concentration of the exposed SD sequence for each construct. Curves were generated with the experimentally determined values of K_a and K_{ISO} and using a relative accessibility of SD in the $PRIMED_{SMK}$ form α, which is estimated to be 0.1. The equilibrium between the ISO_{SMK} conformation and the $PRIMED_{SMK}$ conformation (1) shifts the affinity of the riboswitch into the biologically relevant micromolar range and (2) amplifies the response of the switch to SAM by promoting greater SD accessibility at low [SAM].

and functional data obtained from *in vivo* reporter assays.

First, we note that the 8 nt that distinguish the switchable S_{MK}59 from the switching-incompetent S_{MK}51 shift the affinity of the aptamer for SAM from ~60 nM (S_{MK}51) to ~400 nM (S_{MK}59), closer to the physiologically relevant micromolar concentrations of the metabolite under repressing conditions[17,26,27] (Fig. 4a). Second, the response of the riboswitch is determined by its affinity for SAM and by the exposure of the SD sequence in the accessible conformations of the RNA. The NMR data presented here indicate that the SAM-free states of the S_{MK} box riboswitch, ISO_{SMK} and $PRIMED_{SMK}$, are not equivalent in terms of the accessibilities of their SD sequences (Fig. 6a).

In order to better understand the role of ISO_{SMK} in translation regulation, we considered the effect of the ISO_{SMK}–$PRIMED_{SMK}$ equilibrium on both SAM binding affinity and the concentration of exposed ribosome binding sites $[SD]_{free}$. If the SD sequence is fully exposed in ISO_{SMK} and α represents the relative accessibility of the SD sequence in $PRIMED_{SMK}$, the SAM dependence of the fractional exposure *f* of the

SD sequence can be written as follows (see Supplemental Results):

$$f = \frac{[\mathrm{ISO_{SMK}}] + \alpha[\mathrm{PRIMED_{SMK}}]}{[\mathrm{ISO_{SMK}}] + [\mathrm{PRIMED_{SMK}}] + [\mathrm{BOUND_{SMK}}]} = \frac{K_{\mathrm{ISO}} + \alpha}{K_{\mathrm{ISO}} + 1 + K_a[\mathrm{SAM}]} \quad (3)$$

In this model, the equilibrium between two SAM-free RNA conformations has two effects (Fig. 6c): (1) the competing equilibrium defined by K_{ISO} decreases the effective affinity of the SAM aptamer; and (2) the increased exposure of the SD sequence in the ISO form results in a greater amplitude change in the translational regulatory signal than that achieved by simply destabilizing helix P1 and leaving the SD largely occluded. These expectations are consistent with *in vivo* reporter assays (Fig. 4c), which show that despite its less robust ability to repress gene expression when SAM pools are high (S_{MK}59, 3.0 Miller units; S_{MK}51, 0.34 Miller units), the S_{MK}59 construct is more responsive to reduction in SAM pools as its induction ratio (13-fold) is greater than that of the S_{MK}51-like construct (11-fold) (Fig. 6b). The differential between induction ratios is more pronounced when comparing the naturally occurring S_{MK} box sequence with its P0-incompetent partner (induction ratios of 5.8 and 3.1 for fusion constructs S_{MK}13–116 and S_{MK}20–116, respectively), underscoring the functional importance of an SD-exposing conformational isomer. Similar analyses have been performed with respect to the kinetics of ligand-binding aptamer RNAs,[28,29] although those systems lack the context of a corresponding regulatory element and therefore differ from the present characterization of the S_{MK} box.

Prior studies of the ligand-free aptamer domains of other riboswitches have revealed a variety of structural responses, the most extreme of which parallels the structural changes that we observed with the truncated S_{MK}51 (i.e., the absence of ligand results in destabilization of secondary structural elements). Our thermodynamic analysis and *in vivo* results demonstrate that such an RNA can still operate as a switch; however, the response of this system is inferior to that of a switch that populates two mutually exclusive folds (e.g., ISO and BOUND), enabling both greater gene expression in the absence of SAM and a larger range of SAM-dependent responses that can be titrated to the physiologically relevant flux in SAM pools.

Taken together, these results provide insight into the fine-tuning implicit in the evolution of an effective metabolite-responsive RNA element. For transcriptional riboswitches, the fate of the mRNA is kinetically determined during transcription; thus, thermodynamics is of less importance.[1] In contrast, the S_{MK} box is a translationally controlled RNA element that acts via a thermodynamic (i.e., reversible) mechanism. The half-life of the *metK* mRNA *in vivo* (~3 min) exceeds the half-life of the RNA–SAM complex *in vitro* (~8 s), and switching between the bound form and the free form can be observed *in vitro* on a physiologically relevant timescale.[27] This suggests that a single transcript may have multiple opportunities for the binding and release of SAM and, therefore, multiple opportunities for the regulation of gene expression, underscoring the significance of the two interconverting folds observed in the present study.

The S_{MK} box is particularly amenable to structural study due to its compact nature with overlapping aptamer and regulatory domains. This property has enabled the first detailed insights into the interconverting structures unique to this switchable RNA molecule in both its ligand-bound state and its ligand-free state. Its interdependent structural and regulatory transitions nevertheless obey the same principles at work in larger extended riboswitches, and the present mechanistic framework for interpreting the transitions inherent to riboswitch function (Fig. 6c) should aid in understanding and engineering this class of regulatory RNAs.

Methods

Sample preparation

The full details of RNA transcription and purification are available in Supplemental Methods. Briefly, the S_{MK} leader sequence was positioned downstream of a T7 RNA polymerase promoter between two ribozyme sequences, which allowed preparation of RNA constructs with homogeneous termini corresponding to sequences depicted in Fig. 1. The RNA was transcribed *in vitro*, followed by ribozyme cleavage and denaturing PAGE purification, to remove ribozyme fragments. Anion-exchange chromatography was performed to remove contaminating acrylamide, and the RNA was precipitated with 75% ethanol and 0.3 M NaOAc (pH 5.2). The RNA was resuspended in NMR buffer [25 mM potassium phosphate (pH 6.2), 50 mM NaCl, and 5 mM $MgCl_2$], dialyzed against the same buffer, and stored at −20 °C. Before use, the samples were folded by incubating at 65 °C for 5 min, followed by slow cooling to 4 °C.

Model RNAs (5′-GUUACAGAAAUGUAAC-3′ and 5′-GCUACAGAAAUGUAGC-3′) were purchased from Dharmacon (Fisher Scientific) and used for the confirmation of helix P0 resonance assignment in SAM-free S_{MK}59. To aid the assignment of resonances in SAM-bound S_{MK}51, we introduced paired point sequence alterations to the model RNAs at helix P1 (C22G and G92C) and helix P2 (G30C and C68G).

NMR spectroscopy

Samples (0.5–1.0 mM) were dialyzed into NMR buffer containing 10% D_2O. SAM-bound samples were prepared

by mixing a 10% stoichiometric excess of the ligand from a 5 mM stock solution prepared in NMR buffer. Spectra were recorded at 4 °C, 15 °C, or 25 °C on 600-MHz and 800-MHz Bruker Avance DRX spectrometers (Bruker Avance, Billerica, MA) equipped with triple-resonance pulsed-field *z*-axis gradient cryogenic probes. Pulse sequences [1D: ^{1}H; 2D: NOESY, ^{1}H–^{15}N heteronuclear single-quantum coherence (HSQC), and HNN-COSY[30]] were employed with WATERGATE or flipback water suppression.[31] Homonuclear NOESY spectra used to determine imino proton connectivities were recorded with a mixing time of 300 ms, with 256 complex points in the indirect dimension. ^{1}H–^{15}N HSQC spectra were recorded with 64 complex points in the indirect dimension. HNN-COSY spectra used a 30 ms ^{15}N–^{15}N COSY transfer period, with 32 complex points in the indirect dimension. Spectra were processed using sine bell or Gaussian apodization, with zero-filling once in each dimension. NMRPipe[32] and NMRView[33] were used for processing and analysis, respectively.

Isothermal titration calorimetry

S_{MK}51 and S_{MK}59 RNA samples (typically ≤10 ml) were dialyzed for at least 24 h in total against at least three 0.5-l to 1.0-l volumes of NMR buffer. The final dialysate was used to dissolve crystalline SAM (no. A7007; Sigma-Aldrich), creating a 5 mM stock solution (based on formula weight) that was subsequently diluted to a concentration of 250 μM using the same dialysate. RNA concentrations were estimated by absorbance at 260 nm to be 18.2 μM and 13.6 μM for S_{MK}51 and S_{MK}59, respectively. ITC experiments were performed using a VP-ITC instrument (Microcal) at 15 °C, with a reference power of 15 μcal s^{-1}. For each experiment, we performed fifty 5-μl injections of SAM into the 1.4-ml cell containing the RNA, with a duration of 8.5 s per injection and with 300-s spacing. Experiments were performed in triplicate for both S_{MK}51 and S_{MK}59. The first injection was discarded, and the data from each experiment were fitted to a single-site binding model using Origin (v7.0383; Microcal). Upon fitting, the obtained RNA/SAM stoichiometries slightly less than 1:1 revealed that the active SAM concentration in the syringe was less than expected and decreased between individual runs. This is consistent with the ~80% purity of commercially available SAM and its routinely observed degradation when dissolved in water.[34,35] To correct for this and to ensure a proper fit of the other parameters, we allowed the effective concentration of SAM to vary during fitting from 180 μM to 250 μM, and we assumed a stoichiometry of 1, which is expected based on the S_{MK} box crystal structure[10] and is consistent with the NMR-based observations (data not shown). S_{MK}59 thermograms exhibit a small reproducible feature within the first few injections; this may be due to a minor conformation of the RNA that is otherwise undetected via NMR experiments or via native and denaturing PAGE analysis.

Translational fusions and β-galactosidase assays

Full-length and truncated *E. faecalis metK* leader sequences (see Supplemental Fig. 1), including the first 15 nt of the coding region, were positioned downstream of a *B. subtilis glyQS* promoter (P_{gly}) and fused to codon 18 of a *lacZ* reporter in plasmid pFG328.[36] Constructs were integrated in single copy into the chromosome of *B. subtilis* strain BR151 (*metB10 lys-3 trpC2*) using specialized transducing phage SPβ, as previously described.[36,37] Strains containing *lacZ* translational fusions were selected using chloramphenicol (5 μg ml^{-1}). Cells were grown by shaking at 37 °C in Spizizen minimal media[38] containing methionine (50 μg ml–^{1}) until the early exponential phase. Cells were harvested by centrifugation at 6000***g*** and resuspended in Spizizen minimal media with or without methionine (50 μg ml^{-1}). Aliquots were collected after 4 h of growth at 37 °C and used to measure β-galactosidase activity after the permeabilization of the cells with toluene.[39] β-Galactosidase activity assays were carried out at least in triplicate, and standard deviations are reported.

Small-angle X-ray scattering

SAXS data for S_{MK}51 and S_{MK}59 samples were acquired at beamline 12.3.1 of the Advanced Light Source at Lawrence Berkeley National Laboratory. The samples were passed through a 0.22-μm filter before data acquisition. RNA concentrations varied between 1 mg ml^{-1} and 20 mg ml^{-1}, and NMR buffer was used (with omission of $MgCl_2$ as variable). Data collection was performed at 22 °C. Buffer-only data sets were collected and used for buffer subtraction from the RNA data sets. Exposures of 10 s were collected for interpretation, while 1-s exposures were collected before and after to test for possible radiation damage and to report on intensities in the low-q range (<0.1 $Å^{-1}$). Radiation-damaged samples were not included in the analysis. For each sample, data were collected for RNA concentrations covering an order of magnitude. Data sets were excluded from the analysis if the minimum-concentration and maximum-concentration scattering profiles were not superimposable.

Scattering intensity I was obtained as a function of momentum transfer q in the range $0.02<q<0.32$ $Å^{-1}$. PRIMUS was used to generate Guinier plots, which were used to check for aggregation and to obtain the radius of gyration (Supplemental Fig. 9).[40,41] Kratky plots were generated in Excel (Fig. 5a and b). The program GNOM was used to generate histograms of intramolecular distances $P(r)$ by regularized transformation of scattering intensity.[42] The maximum intramolecular distance D_{max} is provided as an input parameter to GNOM and was initially estimated by setting the value to several hundred angstroms in order to reveal the point at which the upper-limit edge of the histogram nears zero. This initial estimate was then varied until the best fit of the data had been obtained.

The program DAMMIN was used to generate three-dimensional bead models based on the SAXS data of S_{MK}51 bound to SAM.[43] The program was run in "slow" mode, with the model built within a virtual prolate cylinder of 45 Å × 130 Å. Ten independent DAMMIN runs were performed; the resulting models were aligned using SUPCOMB and averaged using DAMAVER.[44,45] The resulting model was aligned to the previously determined

X-ray structure of the S_{MK} box[10] using the program MASSHA[46] and visualized using PyMOL.[47]

Acknowledgements

The authors thank the members of the Foster and Henkin laboratories for invaluable discussions; Michal Hammel (Lawrence Berkeley National Laboratory/SIBYLS Beamline), Elihu Ihms, and the Ohio State University Campus Chemical Instrument Center staff for assistance with data collection; and Harald Schwalbe (Frankfurt University) for helpful discussions on experimental design. This work was funded by National Institutes of Health grant GM063615 (to T.M.H.) and American Recovery and Reinvestment Act supplement GM063615S1 (T.M.H. and M.P.F.) and GM077234 (to M.P.F.). R.C.W. was supported, in part, by a predoctoral fellowship from the American Heart Association.

Supplementary Data

Supplementary data associated with this article can be found, in the online version, at doi:10.1016/j.jmb.2010.10.056

References

1. Garst, A. D. & Batey, R. T. (2009). A switch in time: detailing the life of a riboswitch. *Biochim. Biophys. Acta*, **1789**, 584–591.
2. Henkin, T. M. (2008). Riboswitch RNAs: using RNA to sense cellular metabolism. *Genes Dev.* **22**, 3383–3390.
3. Smith, A. M., Fuchs, R. T., Grundy, F. J. & Henkin, T. M. (2010). Riboswitch RNAs: regulation of gene expression by direct monitoring of a physiological signal. *RNA Biol.* **7**, 104–110.
4. Miranda-Rios, J. (2007). The THI-box riboswitch, or how RNA binds thiamin pyrophosphate. *Structure*, **15**, 259–265.
5. Sudarsan, N., Barrick, J. E. & Breaker, R. R. (2003). Metabolite-binding RNA domains are present in the genes of eukaryotes. *RNA*, **9**, 644–647.
6. Corbino, K. A., Barrick, J. E., Lim, J., Welz, R., Tucker, B. J., Puskarz, I. *et al.* (2005). Evidence for a second class of *S*-adenosylmethionine riboswitches and other regulatory RNA motifs in alpha-proteobacteria. *Genome Biol.* **6**, R70.
7. Fuchs, R. T., Grundy, F. J. & Henkin, T. M. (2006). The S_{MK} box is a new SAM-binding RNA for translational regulation of SAM synthetase. *Nat. Struct. Mol. Biol.* **13**, 226–233.
8. McDaniel, B. A., Grundy, F. J., Artsimovitch, I. & Henkin, T. M. (2003). Transcription termination control of the S box system: direct measurement of *S*-adenosylmethionine by the leader RNA. *Proc. Natl Acad. Sci. USA*, **100**, 3083–3088.
9. Gilbert, S. D., Rambo, R. P., Van Tyne, D. & Batey, R. T. (2008). Structure of the SAM-II riboswitch bound to *S*-adenosylmethionine. *Nat. Struct. Mol. Biol.* **15**, 177–182.
10. Lu, C., Smith, A. M., Fuchs, R. T., Ding, F., Rajashankar, K., Henkin, T. M. & Ke, A. (2008). Crystal structures of the SAM-III/S_{MK} riboswitch reveal the SAM-dependent translation inhibition mechanism. *Nat. Struct. Mol. Biol.* **15**, 1076–1083.
11. Montange, R. K. & Batey, R. T. (2006). Structure of the *S*-adenosylmethionine riboswitch regulatory mRNA element. *Nature*, **441**, 1172–1175.
12. Fuchs, R. T., Grundy, F. J. & Henkin, T. M. (2007). *S*- Adenosylmethionine directly inhibits binding of 30S ribosomal subunits to the S_{MK} box translational riboswitch RNA. *Proc. Natl Acad. Sci. USA*, **104**, 4876–4880.
13. Jucker, F. M., Heus, H. A., Yip, P. F., Moors, E. H. & Pardi, A. (1996). A network of heterogeneous hydrogen bonds in GNRA tetraloops. *J. Mol. Biol.* **264**, 968–980.
14. Rudisser, S. & Tinoco , I., Jr (2000). Solution structure of cobalt(III)hexamine complexed to the GAAA tetraloop, and metal-ion binding to G·A mismatches. *J. Mol. Biol.* **295**, 1211–1223.
15. Monod, J., Wyman, J. & Changeux, J. P. (1965). On the nature of allosteric transitions: a plausible model. *J. Mol. Biol.* **12**, 88–118.
16. Eftink, M. R., Anusiem, A. C. & Biltonen, R. L. (1983). Enthalpy–entropy compensation and heat capacity changes for protein–ligand interactions: general thermodynamic models and data for the binding of nucleotides to ribonuclease A. *Biochemistry*, **22**, 3884–3896.
17. Tomsic, J., McDaniel, B. A., Grundy, F. J. & Henkin, T. M. (2008). Natural variability in *S*-adenosylmethionine (SAM)-dependent riboswitches: S-box elements in *Bacillus subtilis* exhibit differential sensitivity to SAM *in vivo* and *in vitro*. *J. Bacteriol.* **190**, 823–833.
18. Serganov, A., Huang, L. & Patel, D. J. (2008). Structural insights into amino acid binding and gene control by a lysine riboswitch. *Nature*, **455**, 1263–1267.
19. Garst, A. D., Heroux, A., Rambo, R. P. & Batey, R. T. (2008). Crystal structure of the lysine riboswitch regulatory mRNA element. *J. Biol. Chem.* **283**, 22347–22351.
20. Ottink, O. M., Rampersad, S. M., Tessari, M., Zaman, G. J., Heus, H. A. & Wijmenga, S. S. (2007). Ligand-induced folding of the guanine-sensing riboswitch is controlled by a combined predetermined induced fit mechanism. *RNA*, **13**, 2202–2212.
21. Noeske, J., Buck, J., Furtig, B., Nasiri, H. R., Schwalbe, H. & Wohnert, J. (2007). Interplay of 'induced fit' and preorganization in the ligand induced folding of the aptamer domain of the guanine binding riboswitch. *Nucleic Acids Res.* **35**, 572–583.
22. Buck, J., Furtig, B., Noeske, J., Wohnert, J. & Schwalbe, H. (2007). Time-resolved NMR methods resolving ligand-induced RNA folding at atomic resolution. *Proc. Natl Acad. Sci. USA*, **104**, 15699–15704.
23. Serganov, A., Polonskaia, A., Phan, A. T., Breaker, R. R. & Patel, D. J. (2006). Structural basis for gene regulation by a thiamine pyrophosphate-sensing riboswitch. *Nature*, **441**, 1167–1171.

24. Lang, K., Rieder, R. & Micura, R. (2007). Ligand-induced folding of the *thiM* TPP riboswitch investigated by a structure-based fluorescence spectroscopic approach. *Nucleic Acids Res.* **35**, 5370–5378.
25. Stoddard, C. D., Montange, R. K., Hennelly, S. P., Rambo, R. P., Sanbonmatsu, K. Y. & Batey, R. T. (2010). Free state conformational sampling of the SAM-I riboswitch aptamer domain. *Structure*, **18**, 787–797.
26. Wabiko, H., Ochi, K., Nguyen, D. M., Allen, E. R. & Freese, E. (1988). Genetic mapping and physiological consequences of *metE* mutations of *Bacillus subtilis*. *J. Bacteriol.* **170**, 2705–2710.
27. Smith, A. M., Fuchs, R. T., Grundy, F. J. & Henkin, T. M. (2010). The SAM-responsive S_{MK} box is a reversible riboswitch. *Mol. Microbiol.* doi:10.1111/j.1365-2958.2010.07410.x.
28. Jucker, F. M., Phillips, R. M., McCallum, S. A. & Pardi, A. (2003). Role of a heterogeneous free state in the formation of a specific RNA–theophylline complex. *Biochemistry*, **42**, 2560–2567.
29. Gilbert, S. D., Stoddard, C. D., Wise, S. J. & Batey, R. T. (2006). Thermodynamic and kinetic characterization of ligand binding to the purine riboswitch aptamer domain. *J. Mol. Biol.* **359**, 754–768.
30. Dingley, A. J., Nisius, L., Cordier, F. & Grzesiek, S. (2008). Direct detection of N–H[…]N hydrogen bonds in biomolecules by NMR spectroscopy. *Nat. Protoc.* **3**, 242–248.
31. Liu, M., Mao, X., Ye, C., He, H., Nicholson, J. K. & Lindon, J. C. (1998). Improved WATERGATE pulse sequences for solvent suppression in NMR spectroscopy. *J. Magn. Reson.* **132**, 125–129.
32. Delaglio, F., Grzesiek, S., Vuister, G. W., Zhu, G., Pfeifer, J. & Bax, A. (1995). NMRPipe: a multidimensional spectral processing system based on UNIX pipes. *J. Biomol. NMR*, **6**, 277–293.
33. Johnson, B. A. (2004). Using NMRView to visualize and analyze the NMR spectra of macromolecules. *Methods Mol. Biol.* **278**, 313–352.
34. Parks, L. W. & Schlenk, F. (1958). The stability and hydrolysis of *S*-adenosylmethionine; isolation of *S*-ribosylmethionine. *J. Biol. Chem.* **230**, 295–305.
35. Desiderio, C., Cavallaro, R. A., De Rossi, A., D'Anselmi, F., Fuso, A. & Scarpa, S. (2005). Evaluation of chemical and diastereoisomeric stability of *S*-adenosylmethionine in aqueous solution by capillary electrophoresis. *J. Pharm. Biomed. Anal.* **38**, 449–456.
36. Grundy, F. J. & Henkin, T. M. (1993). tRNA as a positive regulator of transcription antitermination in *B. subtilis*. *Cell*, **74**, 475–482.
37. Grundy, F. J. & Henkin, T. M. (1998). The S box regulon: a new global transcription termination control system for methionine and cysteine biosynthesis genes in Gram-positive bacteria. *Mol. Microbiol.* **30**, 737–749.
38. Anagnostopoulos, C. & Spizizen, J. (1961). Requirements for transformation in *Bacillus subtilis*. *J. Bacteriol.* **81**, 741–746.
39. Miller, J. (1972). *Experiments in Molecular Genetics.* Cold Spring Harbor Laboratory Press, Cold Spring Harbor, NY.
40. Guinier, A. & Fournet, G. (1955). *Small-Angle Scattering of X-rays*. Wiley, New York, NY.
41. Konarev, P. V., Volkov, V. V., Sokolova, A. V., Kochb, M. H. J. & Svergun, D. I. (2003). PRIMUS: a Windows PC-based system for small-angle scattering data analysis. *J. Appl. Crystallogr.* **36**, 1277–1282.
42. Konig, S., Svergun, D. I., Koch, M. H., Hubner, G. & Schellenberger, A. (1992). Synchrotron radiation solution X-ray scattering study of the pH dependence of the quaternary structure of yeast pyruvate decarboxylase. *Biochemistry*, **31**, 8726–8731.
43. Svergun, D. I. (1999). Restoring low resolution structure of biological macromolecules from solution scattering using simulated annealing. *Biophys. J.* **76**, 2879–2886.
44. Kozin, M. & Svergun, D. I. (2001). Automated matching of high and low resolution structural models. *J. Appl. Crystallogr.* **34**, 33–41.
45. Volkov, V. V. & Svergun, D. I. (2003). Uniqueness of ab initio shape determination in small-angle scattering. *J. Appl. Crystallogr.* **36**, 860–864.
46. Konarev, P. V., Petoukhov, M. V. & Svergun, D. I. (2001). MASSHA—a graphics system for rigid-body modelling of macromolecular complexes against solution scattering data. *J. Appl. Crystallogr.* **34**, 527–532.
47. DeLano, W. L. (2002). The PyMOL Molecular Graphics System, vol. 2009 DeLano Scientific, San Carlos, CA.